IEEE Access
Multidisciplinary | Rapid Review | Open Access Journal

Received January 6, 2018, accepted March 20, 2018, date of publication March 23, 2018, date of current version April 23, 2018.

Digital Object Identifier 10.1109/ACCESS.2018.2818756

Day-Ahead Scheduling of Distribution Level Integrated Electricity and Natural Gas System Based on Fast-ADMM With Restart Algorithm

JIAN CHEN[1], (Member, IEEE), WEITONG ZHANG[1], (Student Member, IEEE), YICHENG ZHANG[2], (Student Member, IEEE), AND GUANNAN BAO[3]

[1]Key Laboratory of Power System Intelligent Dispatch and Control of Ministry of Education, Shandong University, Jinan 250061, China
[2]School of Electrical and Electronic Engineering, Nanyang Technological University, Singapore 639798
[3]State Grid Shandong Electric Power Dispatching and Control Center, Jinan 250001, China

Corresponding author: Jian Chen (ejchen@sdu.edu.cn)

This work was support by the National Natural Science Foundation of China under Grant 51507094.

ABSTRACT Power generated by the natural gas (NG) is a promising option for solving the restrictions on the development of the power industry. Consequently, the high interdependence between NG network and electricity network should be considered in this integration. In this paper, a day-ahead scheduling framework of integrated electricity and NG system (IENG) is proposed at a distribution level based on the fast alternating direction multiplier method with restart algorithm considering demand side response and uncertainties. Within the proposed framework, the detailed model of the IENG system at a distribution level is established, where the NG flow equation is processed by incremental linearization method to improve the computational efficiency. The objective is to minimize the operation costs of the entire system. With consideration of the uncertainties of distributed generation and electricity load as well as the uncertainties from the NG load, a two-stage robust optimization model is introduced to obtain the worst case within the uncertainty set, which is solved by column and constraints generation algorithm. In addition, the demand-side response (DSR) model including the decentralized air conditioning (AC) load model and the centralized ice-storage AC load model is integrated into the scheduling framework. Finally, the proposed day-ahead scheduling framework is verified by numerical studies where the optimal scheduling schemes are obtained in different cases, both the effects of the uncertainties and the performance with introducing DSR to the system operation are analyzed.

INDEX TERMS Day-ahead scheduling, demand-side response (DSR), integrated electricity and natural gas system (IENG), natural gas (NG), uncertainty.

I. INTRODUCTION

Environmental degradation and fossil energy depletion are the main factors which limit the development of the power industry. To solve these issues and sequentially promote the development of the power industry, the utilization of natural gas (NG) has been paid more and more attention due to its low-cost and high environmental benefits [1], [2]. Currently, the generation units utilizing NG like micro-turbine (MT) are becoming a top priority in electricity systems. Moreover, the large-scale configuration of MT is bound to result in the high interdependence between NG network and electricity network [3].

For an integrated energy system involving electricity and NG network, the view of 'source-grid-load' coordinated optimization is required to find the best scheduling scheme with the minimum overall cost in the whole system [4]. Due to the interdependence of electricity network and NG network, optimizing either of the system and neglecting the interaction between them may result in the increase of operation costs from the system point of view. Consequently, a joint optimization is more effective for IENG [5]–[7]. An IENG planning algorithm is proposed to enhance the power grid resilience in extreme conditions which is described by the proposed variable uncertainty set [8]; a multi-objective framework is proposed for the coordinated operation of the IENG, addressing the economic, dynamic security of electricity network, as well as the security of the NG network [9]. However, most previous investigations focus

on the issues of interactions between electricity and NG networks at a transmission level rather than at a distribution level [10]. With the large access of MT in distribution network, the interdependence of distribution network and NG network should be considered. Moreover, significant differences exist in the models of the IENG system regarding the distribution and transmission levels. Firstly, the network structure, parameters and power flow algorithm of the transmission network are different from those of the distribution network; secondly, the transmission network of NG have long distance pipelines and large amount of NG which lead to a large pressure loss of pipelines and compressors are required to compensate the loss of pressure [11], while the loss of pressure at a distributed level is much lower where compressors are not necessary. Due to these differences, it is essential to establish a detailed model of the IENG at a distribution level and to investigate the scheduling problem.

Besides, the IENG system is always formulated as a large-scale mixed integer nonlinear programming problem in which the nonlinearity of the NG flow equation is the key computational bottleneck. In [12], the pressure of pipeline is ignored during operation process. In order to expedite the solving process, the natural gas pipeline flow is represented as a variable constrained with pipeline capacity at each period in [13]. Reference [14] proposes the method of the IENG joint planning so that the gas turbines are reasonably connected to the distribution network, and the intelligent algorithm is used to solve this problem. However, the model which ignores the pressure of pipelines may result in that the planning results do not match the actual results. In the model of [14], intelligent algorithms are normally adopted to obtain the solutions, which cannot guarantee the optimal solution. Therefore, considering the accuracy and efficiency, the linearization is required to simplify the nonlinear flow equations which can effectively tackle the shortcomings of existing models within the tolerable range [15].

For the sources in the electricity system, the uncertainty of DG should be considered because of intermittent of renewable energy [16], [17]. Reference [18] proposes a robust co-optimization scheduling model to minimize the total costs of the electricity sub-system and NG sub-system considering power system uncertainty. Except the uncertainty of sources, the fluctuations of load (including gas turbines, MT, household load, etc.) also have a great impact on the operation of the entire system especially at a distribution level. In [19] and [20], the Monte Carlo simulation is applied to create multiple scenarios for representing the coordinated system uncertainties including the uncertainty of NG load. However, the scheduling schemes obtained by the scenarios approach may be infeasible in the extremely case. As a result, it is essential to consider the impact of NG load uncertainty and deal with it by robust methods.

In addition to the uncertainty of load, DSR can offer an effective option to reduce system operation costs and stabilize the power fluctuations [21], [22]. Currently, the proportion of air conditioning (AC) load in the total load has been gradually increasing which even reach 30%-40% in the summer [23], and a number of control methods create the conditions for participation of AC in the DSR. As an important DSR resource, the AC load can respond quickly to the power dispatching through the reasonable regulation, which can effectively alleviate the contradiction between power supply and demand and reduce the system peaking difficulty and operation cost. Reference [24] proposes a microgrid optimization scheduling model considering the centralized ice-storage AC load, which reduces the operation cost of the system by utilizing the shifting characteristics of ice-storage AC load. The periodic suspension control strategy of decentralized AC load is proposed in [25], and the indoor temperature is controlled within a certain range according to the heat storage characteristics of the building. Centralized AC load is generally concentrated in the daytime when scheduling potential is high, but the scheduling potential at night is very low. Decentralized AC load peak load generally appears in the evening, and valley load appears in the morning, so that decentralized AC load have higher scheduling potential in peak period than that in valley period. Since the scheduling potentials of the two AC loads vary in different periods, considering the two kinds of AC loads can play a complementary role, which is rarely concerned with the current researches. To further reduce the system operation costs and power fluctuations, it is worth to note the complementary effect of the different AC loads.

To realize an integrated management of the IENG at a distribution level, a detailed IENG model at a distribution level is established in the paper. Firstly, the electricity network model is described by simplified Dist-flow equations, and an incremental linearization method is used to simplify the NG flow equation. Secondly, the uncertainties of DG are considered because of the intermittent of renewable energy. Furthermore, the uncertainties of load are considered including both electricity load and NG load, and a two-stage robust optimization model (TSRO) model is introduced where the worst case is obtained by C&CG algorithm. In addition, hourly demand response of AC load is considered. According to different control methods, decentralized AC load model and centralized ice-storage AC load model are proposed, respectively. Finally, an optimization framework of the IENG is proposed based on fast-ADMM with restart algorithm which tackles the information barriers between the different operators. The main contributions of this paper can be summarized as follows: (1) The impacts of uncertainties including NG load uncertainty on the system are considered, which is formulated as a TSRO problem and solved by C&CG algorithm; (2) The DSR model of decentralized AC load and centralized ice-storage AC load is established; (3) The model of IENG at a distribution level based on fast-ADMM with restart algorithm is established which offers higher convergence accuracy within limited iteration times.

The paper is organized as follows. Section II describes the mathematical model of the system. Section III introduces the formulation of uncertainty. Section IV formulates the optimization problem. Finally, optimization results of case

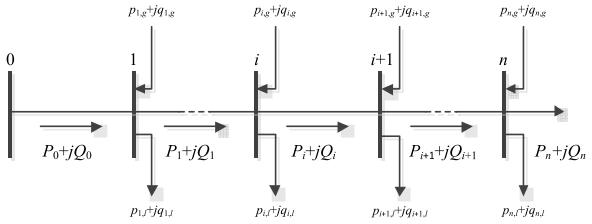

FIGURE 1. The radial distributed network.

study and conclusions are presented in Section V and VI, respectively.

II. MODEL OF IENG AT A DISTRIBUTION LEVEL

In this section, the detailed models of IENG are proposed, including the economic model and the operation model.

A. ECONOMIC MODEL OF IENG

The objective function describes the economic costs of the entire system, including the electricity system costs $Cost'_{grid}$, the startup/shutdown costs of MT C_{MT} and the NG system costs $Cost'_{gas}$. Among them, the cost of electricity system includes the purchase costs from main grid, electricity sales revenue to main grid; and NG system costs include NG production costs and NG storage costs.

$$MinCost'_{grid} + Cost'_{gas} + C_{MT} \tag{1}$$

$$Cost'_{grid} = \sum_{t=1}^{T} [P_{in}(t)\, C_{ele.purchase}(t) - P_{out}(t)\, C_{ele.sell}(t)] \tag{2}$$

$$Cost'_{gas} = \sum_{t=1}^{T} [F_{supply}(t)\, C_{gas.supply}(t) + F_{in}(t)\, C_{gas,inject}(t)] \tag{3}$$

where T is the day-ahead scheduling period; t represents the time; P_{in} is the power transferred from main grid to distribution network; P_{out} is the power transferred from distribution network to main grid; F_{supply} is the gas supplied by transmission network; F_{in} is the gas injection amount of the gas storage tank; $C_{ele.purchase}$ is the price purchasing from main grid; $C_{ele.sell}$ is the price selling to main grid; $C_{gas.supply}$ is the price purchasing from transmission network; $C_{gas.inject}$ is the storage price of gas storage.

B. OPERATION MODEL OF IENG

1) MODEL OF ELECTRICITY NETWORK

In this paper, traditional radial distributed network is considered which is shown in Figure 1, and Dist-Flow [26] is used to describe the complex power flow.

$$P_{i+1}(t) = P_i(t) - \frac{r_i(P_i^2(t) + Q_i^2(t))}{V_i^2(t)} - p_{i+1,l}(t) + p_{i+1,g}(t) \tag{4}$$

$$Q_{i+1}(t) = Q_i(t) - \frac{x_i(P_i^2(t) + Q_i^2(t))}{V_i^2(t)} - q_{i+1,l}(t) + q_{i+1,g}(t) \tag{5}$$

$$V_{i+1}^2(t) = V_i^2(t) - 2(r_i P_i(t) + x_i Q_i(t)) + \frac{(r_i^2 + x_i^2)[P_i^2(t) + Q_i^2(t)]}{V_i^2(t)} \tag{6}$$

where i represents the node in the distribution network; P_i, Q_i are the active and reactive power of line from node i to $i+1$, respectively; $p_{i,g}$,$q_{i,g}$ are active and reactive power of generation of node i; $p_{i,l}$,$q_{i,l}$ are active and reactive load of node i, respectively; r_i, x_i are resistance and reactance between node i and $i+1$, respectively; V_i is the voltage of node i.

The Dist-Flow equations can be simplified using linearization. The linearized power flow equations have been extensively used and justified in both traditional distribution systems and MGs [27]–[29]. In addition, the voltage level at each node is within the permissible range.

$$P_{i+1}(t) = P_i(t) - p_{i+1,l}(t) + p_{i+1,g}(t) \tag{7}$$

$$Q_{i+1}(t) = Q_i(t) - q_{i+1,l}(t) + q_{i+1,g}(t) \tag{8}$$

$$V_{i+1}(t) = V_i(t) - [r_i P_i(t) + x_i Q_i(t)]/V_0 \tag{9}$$

$$V_i^{min} \le V_i(t) \le V_i^{ma} \tag{10}$$

2) MODEL OF NG NETWORK

NG network constraints [9] are shown in the following equations. The Weymouth equation is employed to describe the relationship between the pressure loss and the natural gas flow in the pipelines as shown in Eq. (11). The flow and node pressure is within certain range due to the physical characteristic of pipelines as shown in Eq. (12)∼(13). Besides, the node demand-supply balance is described by Eq. (14).

$$sign \cdot (fp_q(t))^2 = \varphi(\pi_m^2(t) - \pi_n^2(t))$$

$$sign = \begin{cases} 1, & \pi_m \ge \pi_n \\ -1, & \pi_m < \pi_n \end{cases} \tag{11}$$

$$F_q^{min} \le fp_q^2(t) \le F_q^{max} \tag{12}$$

$$\pi_m^{min} \le \pi_m^2(t) \le \pi_m^{max} \tag{13}$$

$$\sum_{q \in S_m} fp_q(t) + F_{m,s}(t) - F_{m,l}(t) = 0 \tag{14}$$

where q represents the number of pipelines; m or n is the node of NG network; $sign$ is the variable representing the direction of gas flow;fp_q is NG flow of pipe q; φ is NG pipeline parameters; π_m, π_n are the pressure of node m and n, respectively; F_q^{min} and F_q^{max} are the lower and upper limits of NG flow in the pipeline q; π_m^{min} and π_m^{max} are the lower and upper limits of pressure in node m; S_m is the set of pipelines which is attached to node m; $F_{m,s}$ is the gas supply of node m;$F_{m,l}$ is the gas load of node m.

To reduce the computational difficulty, the nonlinear constraints are linearized by the incremental linearization method [15], [30]. The nonlinearity of the square terms of NG

pipeline pressure, π^2, can be eliminated by a new variable $ps_m = \pi_m^2$. In this case, the nonlinear term turns to be the square term of the NG flow, fp^2, then the flow equations are linearized by introducing variables $\delta_{q,k}$ and $\eta_{q,k}$, where $\eta_{q,k}$ are binary variables. The specific linearization process is shown in the following:

1) Balance the linearization accuracy and the calculation amount, then determine appropriate number of linear segments, NP, and calculate the reference point fpq, 1, $fp_{q,2}, \ldots, fp_{q,NP}$ by Eq. (15);
2) Describe $fp_1, fp_2, \ldots, fp_{NP}$ by variables $\delta_{q,k}$ and constants F_q^{min}, F_q^{max} and NP in Eq. (16);
3) Find fp_q^2 values corresponding to each discrete point by the reference point and variables $\delta_{q,k}$ in Eq. (17);
4) Ancillary variables $\delta_{q,k}$ and $\eta_{q,k}$ subjected to constraints Eq. (18)∼(19) are added.

$$fp_{q,k}(t) = F_q^{min} + k\left(F_q^{max} - F_q^{min}\right)/(NP-1), \quad k = 1, 2, \ldots, NP-1 \tag{15}$$

$$fp_q(t) = F_q^{min} + \sum_{k=1}^{NP-1} (F_q^{max} - F_q^{min})/(NP-1)\,\delta_{q,k}(t) \tag{16}$$

$$fp_q^2(t) = fp_{q,1}^2(t) + \sum_{k=1}^{NP-1} [fp_{q,k+1}^2(t) - fp_{q,k}^2(t)]\delta_{q,k}(t) \tag{17}$$

$$\delta_{q,k+1}(t) \le \eta_{q,k}, \eta_{q,k}(t) \le \delta_{q,k}(t), \quad k = 1, 2, \ldots, NP-2 \tag{18}$$

$$1 \le \delta_{q,k}(t) \le 0, \quad k = 1, 2, \ldots, NP-1 \tag{19}$$

3) MODEL OF MT

The annual fuel costs of the MT $C_{gas,fuel}$ can be calculated from the power of MT, P_p^{mt}, by the power consumption function [31]:

$$C_{gas.fuel} = \sum_{t=1}^{T} \alpha + \beta P_p^{mt}(t) + \gamma [P_p^{mt}(t)]^2 \tag{20}$$

where p is the numbers of MT; the parameters, α, β, γ of the consumption function can be chosen from the fuel consumption curve of the MT [32]. The MT also should be subject to the on and off constraints:

$$U_p(t) P_p^{min} \le P_p^{mt}(t) \le U_p(t) P_p^{max} \tag{21}$$

$$I_p(t) + M_p(t) \le 1 \tag{22}$$

$$U_p(t-1) - U_p(t) + I_p(t) - M_p(t) = 0 \tag{23}$$

where U_p is a binary variable describing the state of MT; I_p and M_p are binary variables representing on and off states of MT, respectively; P_p^{min}, P_p^{max} are the lower and upper power limits of MT, respectively.

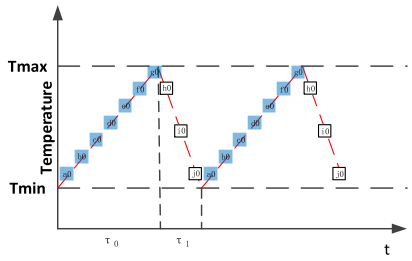

FIGURE 2. The equivalent thermal parameter model.

4) MODEL OF DSR

Owing to the DSR characteristics of AC load, power dispatch can achieve quick response with reasonable control method, which alleviates the contradiction between power supply and demand and reduces operation costs. Due to the distinctive characteristics of the AC load, the control methods are also variant. The AC load considered in this paper includes decentralized AC load and centralized ice-storage AC load.

For decentralized AC, controlling the state of AC can maintain the indoor temperature within a certain range according to the thermal hysteresis effect of the room. As shown in Figure 2, the on time τ_0 and the off time τ_1 can be obtained by thermal parameter model, where the time of a control cycle is τ_c. The AC are divided into τ_c groups and each group has τ_c states. Consequently, when entering the next control cycle, there is always a group of AC to be off, and another group of AC to be on, which guarantee that only τ_1 groups of AC are on for every minute [33].

The specified control method is shown as follows. Assuming the control period of the AC is 10 min, the on time is 3 min, the off time is 7 min. Then every group has 10 states (a_0, b_0, c_0, d_0, e_0, f_0, g_0, h_0, i_0, j_0) as shown in Figure 2. The state distribution of the 10 groups of AC in the two control cycles is shown in Figure 3, where the horizontal axis represents the number of AC groups, and the vertical axis represents the time interval. For every group, the AC are on for 7 min (the states of a_0, b_0, c_0, d_0, e_0, f_0, g_0) and off for 3 min (the states of h_0, i_0, j_0), which ensure the temperature to be maintained in a certain range in each control cycle. Furthermore, for every minute, there are only 3 groups to be on. Therefore, the load of decentralized AC after reduction can be calculated as follows:

$$P_{de}(t) = P_{de0}(t)\,\tau_1/(\tau_0 + \tau_1) = P_{de0}(t)\,a \tag{24}$$

where the P_{de0} represents the original decentralized AC load of corresponding nodes, which is a part of total electric load, $p_{i,l}$; P_{de} represents the AC load after DSR; a is the cut coefficient.

As shown in Figure 4, the ice-storage AC generally includes the chiller unit, ice-storage tank, pumps and other auxiliary equipment and the ice is used as storage medium. Centralized ice-storage AC makes and stores ice in the ice storage tank (ice-making mode) in the evening when the electricity price is low. The ice is melted (ice-melting mode)

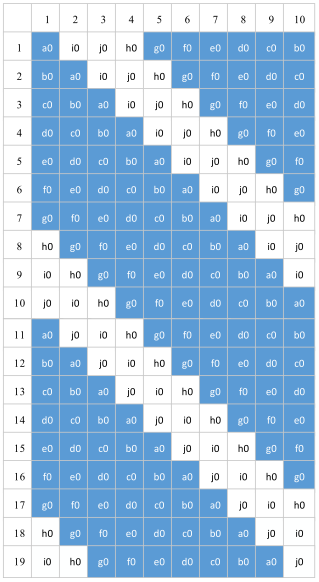

FIGURE 3. The state distribution of AC in the two control cycles.

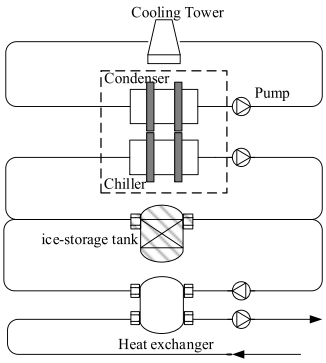

FIGURE 4. The ice-storage AC model.

in the daytime when the electricity price is high, and the chiller operates (cooling-making mode) at the same time to joint supply the cooling load. The system operation costs are reduced in which the load is shifted from high price period to the low price period [34], [35]. Centralized ice-storage AC has two modes of operation: the chiller provides the base load or the ice-storage tank provides the base load. The later makes full use of the ice-storage tank, which results in more benefits than the chiller priority mode. Centralized ice-storage AC load model is as follows: the cooling load supply-demand balance is shown in Eq. (25); the calculation of ice column of ice storage tank is shown in Eq. (26); the relationship between the power consumption of chiller and cooling power is described by Eq. (27); the cooling power of chiller in ice-making mode or cooling-making mode should be in certain range as shown in Eq. (28)∼(29), and the ice-making mode or cooling-making mode cannot operate at the same time in Eq. (30).

$$Q_{load}(t) = Q_a(t) + Q_d(t) \tag{25}$$

$$E_{red}(t) = (1-\theta_1)Q_a(t) + \theta_2 Q_d(t)\,\Delta t - Q_d(t)\,\Delta t \tag{26}$$

$$P_a(t) = Q_a(t)/COP,\ P_c(t) = Q_c(t)/COP \tag{27}$$

$$I_a(t)\,Q_{a-min} \le Q_a(t) \le Q_{a-max} I_a(t) \tag{28}$$

$$I_c(t)\,Q_{a-min} \le Q_c(t) \le Q_{a-max} I_c(t) \tag{29}$$

$$I_a(t) + I_c(t) \le 1 \tag{30}$$

where Q_{load} is the cooling load; E_{red} is the cooling power stored in ice storage tank; P_a represents the electric power of chiller in cooling-making mode; P_c represents the electric power of chiller in ice-making mode; Q_a and Q_c are the cooling power corresponding to the electric power P_a and P_c, respectively; Q_d is the cooling power by melting ice; I_a and I_c are the state variables of cooling-making mode and ice-making mode; Q_{a-min} and Q_{a-max} are lower and upper cooling power of chiller; θ_1 is the dissipation coefficient of stored cooling, which is chosen to be 0.02. θ_2 is refrigeration coefficient, equaling to be 0.67. COP is coefficient of refrigeration of chiller [36].

5) MODEL OF NG STORAGE TANK

The NG load may exceed the capacity of pipelines, but it is not economical to build new NG pipelines. Accordingly, the NG storage facilities serve as adjustable supply or demand entities when the network security or load cannot be guaranteed [37]. The capacity of the storage should be kept at a certain level to ensure an enough pressure of gas storage tank:

$$F_{s,min} \le F_s(t) \le F_{s,max} \tag{31}$$

The gas withdrawal and injection amount are also subject to in-flow and out-flow limit [37]:

$$F_{w,min} \le F_w(t) \le F_{w,max} \tag{32}$$

$$F_{in,min} \le F_{in}(t) \le F_{in,max} \tag{33}$$

Besides, storage capacity is calculated as Eq. (34) at each time step [38].

$$F_s(t+1) = F_s(t) - F_w(t) + F_{in}(t) \tag{34}$$

where F_s is the gas column in gas storage tank; F_w is gas withdrawal amount of gas storage tank; $F_{s,min}$, $F_{s,max}$ are lower and upper limit of gas storage tank, respectively; $F_{w,min}$, $F_{w,max}$ are lower and upper limit of gas withdrawal amount, respectively; $F_{in,min}$, $F_{in,max}$ are lower and upper limit of gas injection amount, respectively.

III. FORMULATION OF UNCERTAINTY

To obtain the robust solution of the system with consideration of uncertainties, a TSRO model is introduced and C&CG algorithm is utilized to solve this problem.

A. TWO-STAGE ROBUST OPTIMIZATION MODEL

In the robust optimization model, uncertainty is grouped as a set, and the uncertainty variables are obtained to represent the worst case. In the worst case, the uncertainty variables are fixed, and the optimal solution obtained in this scenario is the robust solution under uncertainty.

The TSRO model can be formulated as follows in a matrix form:

$$\begin{aligned}&\min_x\{c^T x+\max_u\min_y d^T y\}\\&s.t.\ Ax\geq b,\quad Bx=e,\quad Dy\geq f,\quad Ey=g,\\&Fy\geq -Gx,\quad Jy\leq w,\quad Ky\leq pv,\quad My=l\end{aligned}\tag{35}$$

where x is the first-stage variable as well as the binary vector representing the state variables of MT; u is uncertainty variable set including uncertainty variables w, pv and l; y is the second-stage variable including P_p^{mt}, P_i, Q_i, V_i, fp_q, F_{in}, F_w, π_m, P_w, P_{pv}, P_{load} and F_{load}; P_w, P_{pv}, P_{load} and F_{load} are actual wind power, photovoltaic power, electricity load and NG load; $c^T x$ represents the startup/shutdown costs of MT, C_{MT}; $d^T y$ represents the costs including $Cost'_{grid}$ and $Cost'_{gas}$; A and b, B and e are the corresponding matrix representing the inequality and equality constraints about variables x, respectively. D and f, E and g are the corresponding matrix representing the inequality and equality constraints about variables y. F and G are the corresponding matrix representing the inequality constraints about variables x and y. J, K, M are the corresponding matrix representing the inequality constraints about variables y and uncertain variables w, pv, l. In the TSRO problem shown in Eq. (35), the first '$m$in' aims to minimize the first-stage costs by optimizing the first-stage variable x. The '$m$ax' is to find the worst case under the uncertainty set u by maximizing the minimization of the second stage costs. The second '$m$in' is to minimize the second stage costs by optimizing the second-stage variable y. The uncertainty sets of wind power, photovoltaic power, electricity load and NG load is described as follow:

$$\begin{aligned}U_w=&\{w:P_w(t)=P_{w0}(t)+\mu_+(t)P_{w+}(t)\\&-\mu_-(t)P_{w-}(t)\}\end{aligned}\tag{36}$$

$$\begin{aligned}U_{pv}=&\{pv:P_{pv}(t)=P_{pv0}(t)+\beta_+(t)P_{pv+}(t)\\&-\beta_-(t)P_{pv-}(t)\}\end{aligned}\tag{37}$$

$$\begin{aligned}U_{load}=&\{l:P_{load}(t)=P_{l0}(t)+\theta_+(t)P_{l+}(t)\\&-\theta_-(t)P_{l-}(t)\}\end{aligned}\tag{38}$$

$$\begin{aligned}U_{g,load}=&\{l:F_{load}(t)=F_{l0}(t)+\sigma_+(t)F_{l+}(t)\\&-\sigma_-(t)P_{l-}(t)\}\end{aligned}\tag{39}$$

where U_w, U_{pv}, U_{load} and $U_{g,load}$ are uncertainty set of forecast data; P_{w0}, P_{pv0}, P_{l0} and F_{l0} are forecast data, and P_{w+}, P_{w-}, P_{pv+}, P_{pv-}, P_{l+}, P_{l-}, F_{l+}, F_{l-} represent the positive and negative deviation of forecast data, and μ_+, β_+, θ_+, σ_+, μ_-, β_-, θ_- and σ_- represent the binary variables of deviation. Because of information privacy of different operators, the entire problem is decomposed into two sub-problems according to two different system. Based on above form and variables, the TSRO problems are organized as follow including electricity sub-problem and NG sub-problem.

$$\begin{aligned}&\min_{U_p,I_p,M_p}\ C_{MT}+Cost'_{grid}\\&s.t.\ constraints\ (7)\sim(10),(20)\sim(30),(36)\sim(38)\end{aligned}\tag{40}$$

$$\begin{aligned}&\min_{U_p,I_p,M_p}\ \max_l\ \min_{fp_q,F_{in},F_{load}\atop F_w,\pi_m}\ Cost'_{gas}\\&s.t.\ constraints\ (12)\sim(19),\ (31)\sim(34),(39)\end{aligned}\tag{41}$$

B. COLUMN AND CONSTRINTS GENERATION (C&CG)

For TSRO problem, Benders decomposition and C&CG are widely used. According to [40], the convergence speed and iteration times of C&CG are better than Benders decomposition, and C&CG is selected to solve this problem. In the C&CG algorithm, the TSRO problem (35) is decomposed into the main problem (42) and the slave problem (43).

$$\begin{aligned}&\min_x c^T x+\lambda\\&s.t.\ Ax\geq b,\quad Bx=e,\quad d^T y\geq\lambda\end{aligned}\tag{42}$$

$$\begin{aligned}&\max_u\min_y d^T y\\&s.t.\ Dy\geq f,\quad Ey=g,\quad Fy\geq -Gx,\\&Jy\leq w,\quad Ky\leq pv,\quad My=l\end{aligned}\tag{43}$$

According to above form, the TSRO problem of electricity sub-problem in this paper is organized as follows, which includes the main problem (44) and the slave problem (45).

$$\begin{aligned}&\min_x C_{MT}+\lambda\\&s.t.\ (21)\sim(23),\quad \mathrm{Cost}'_{grid}\geq\lambda\end{aligned}\tag{44}$$

$$\begin{aligned}&\max_{w,pv,l}\ \min_{P_p^{mt},P_i,Q_i,V_i,\atop P_w,P_{pv},P_{load}}\ \mathrm{Cost}'_{grid}\\&s.t.\ (7)\sim(10),(20),(24)\sim(30)\end{aligned}\tag{45}$$

For the 'max-min' slave problem (43), it can be transformed into a 'max' problem by introducing the dual variables which is a bilinear maximization problem and the dual problem can be described as follow [41]:

$$\begin{aligned}&\max_{\alpha',\beta',\chi',\gamma',\psi',\atop\mu',w,p,l}\ \left\{\begin{array}{l}-\alpha'^T f+\beta'^T g-\chi'^T(h-Gx)\\-\gamma'^T w-\psi'^T p+\mu'^T l\end{array}\right\}\\&s.t.\ -\alpha'^T D+\beta'^T E-\chi'^T F-\gamma'^T J-\psi'^T K+\mu'^T M=d^T\\&\alpha'\geq 0,\ \chi'\geq 0,\ \gamma'\geq 0,\ \psi'\geq 0,\ w\in U_w,\ p\in U_{pv},\ l\in U_{load}\end{aligned}\tag{46}$$

where α', β', χ', γ', ψ', μ' are the dual variables of y. However, $\gamma'^T w$, $\psi'^T pv$ and $\mu'^T l$ are bilinear term which is difficult to solve. Therefore, big-M method is used to handle this bilinear problem [42]. The bilinear term, $\gamma'^T w$, is linearized as following:

$$\begin{aligned}\gamma'^T w=&\gamma'(t)P_{w0}(t)+\gamma'(t)\mu_+(t)P_{w+}(t)\\&-\gamma'(t)\mu_-(t)P_{w-}(t)\end{aligned}\tag{47}$$

$$\delta_+(t)=\gamma'(t)\mu_+(t)\tag{48}$$

$$\delta_-(t)=\gamma'(t)\mu_-(t)\tag{49}$$

$$\begin{aligned}&\gamma'(t)-M'[1-\mu_+(t)]\leq\delta_+(t)\\&\leq\gamma'(t)+M'[1-\mu_+(t)]\end{aligned}\tag{50}$$

$$\begin{aligned}&-\gamma'(t)-M'[1-\mu_-(t)]\leq\delta_-(t)\\&\leq-\gamma'(t)+M'[1-\mu_-(t)]\end{aligned}\tag{51}$$

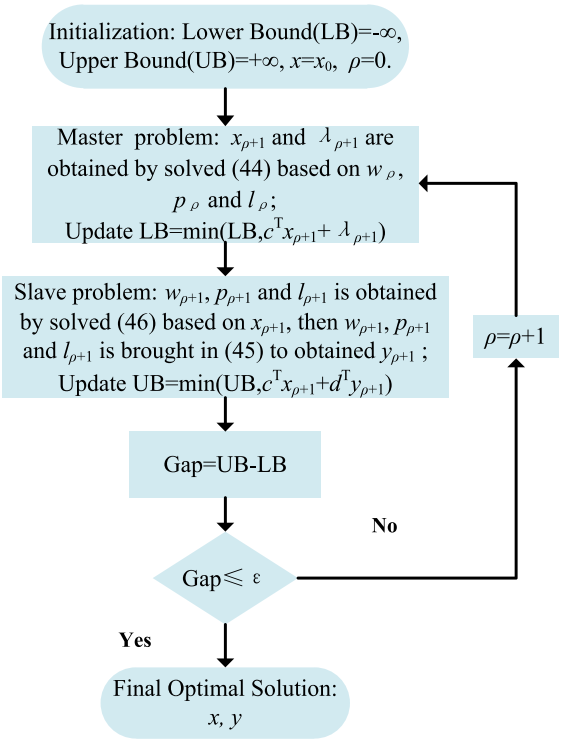

FIGURE 5. The Flowchart of C&CG.

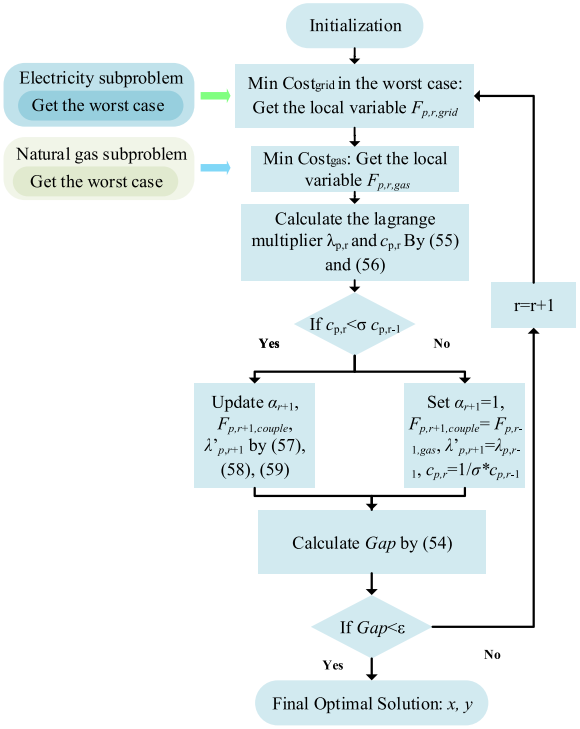

FIGURE 6. Framework of optimal scheduling based on fast-ADMM with restart.

where M' is a large enough constant; $\delta_-(t)$, $\delta_+(t)$ are the auxiliary variables. By Eq. (47)∼(51), the bilinear term is transferred to linear constraints, and $\psi'^T pv$ and $\mu'^T l$ can also be handled in the same method.

The specific flowchart is shown in Figure 5:

Step 1: Initialize lower bound (LB), upper bound (UB). Set $x = x_0$, iteration times $\rho = 0$, initialize w_0, p_0, l_0;

Step 2: $x_{\rho+1}$ and $\lambda_{\rho+1}$ are obtained by solved (44) based on w_ρ, p_ρ and l_ρ, then LB is updated;

Step 3: $w_{\rho+1}$, $p_{\rho+1}$ and $l_{\rho+1}$ is obtained by solved (46) based on $x_{\rho+1}$, then $w_{\rho+1}$, $p_{\rho+1}$ and $l_{\rho+1}$ is brought in (45) to obtained $y_{\rho+1}$ and update the UB;

Step 4: If thresholds, *G*ap, are small enough, the optimal solution is obtained. Otherwise, turn to Step 2.

IV. FORMULATION OF OPTIMIZATION PROBLEM

In this section, an optimal day-ahead scheduling framework for the IENG system at a distributed level is formulated based on the fast-ADMM with restart algorithm. Distributed algorithm is used to guarantee the privacy of their information for operators of electricity and NG systems and adopt distinct models and algorithms to solve their individual systems. The ADMM is well suited to distributed optimization, and in particular to large-scale problems [43]. And the fast-ADMM with restart algorithm use a restart rule can improve the stability of convergence rate [44].

A. OPTIMAL DAY-AHEAD SCHEDULING MODEL BASED ON FAST-ADMM WITH RESTART ALGORITHM

The IENG system includes the electricity network and the NG network, but it is difficult to carry out the optimization over the whole system directly because of the opacity of the information between the two operators. To obtain the optimal solution, the fast-ADMM with restart algorithm is utilized where the entire system is decomposed into an electricity sub-problem and a NG sub-problem, which are iteratively solved. According to the fast-ADMM with restart algorithm, the NG consumption of MT, $F_{p,r,couple}$, represents the linkage between sub-problems of IENG. Besides, $F_{p,r,grid}$ and $F_{p,r,gas}$ are the local variables in the sub-problems corresponding to the global variable $F_{p,r,couple}$.

(1) Electricity Sub-problem

$$Cost_{grid} = Cost'_{grid} + C_{MT} + \sum_{t=1}^{T}\sum_{p}\left\{\begin{array}{l}\lambda'_{p,r}(t)\left[F_{p,r,grid}(t) - F_{p,r,couple}(t)\right] \\ +\left[F_{p,r,grid}(t) - F_{p,r,couple}(t)\right]^2\tau/2\end{array}\right\}$$
$$s.t.\ constraints\ (7)\sim(10),\ (20)\sim(30),\ (36)\sim(38) \quad (52)$$

(2) NG Sub-problem

$$Cost_{gas} = Cost'_{gas} + \sum_{t=1}^{T}\sum_{p}\left\{\begin{array}{l}\lambda'_{p,r}(t)\left[F_{p,r,gas}(t) - F_{p,r,grid}(t)\right] \\ +\left[F_{p,r,gas}(t) - F_{p,r,grid}(t)\right]^2\tau/2\end{array}\right\}$$
$$s.t.\ constraints\ (12)\sim(19),\ (31)\sim(34),\ (39) \quad (53)$$

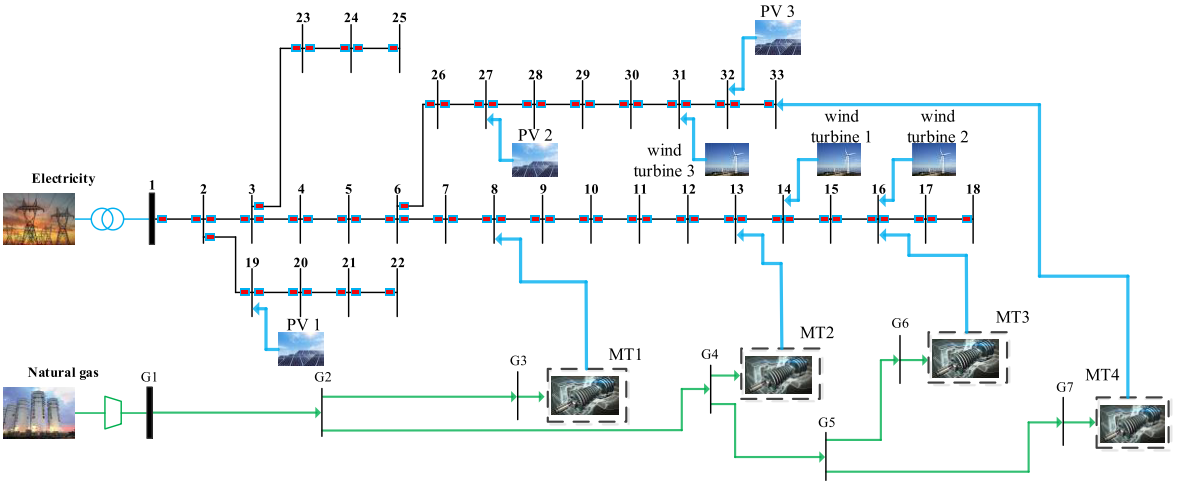

FIGURE 7. IENG system.

B. FRAMEWORK OF THE OPTIMAL SCHEDULING

Based on the fast-ADMM with restart algorithm the framework of optimal scheduling is shown in Figure 6. First, the worst cases are obtained by C&CG based on the objective function and constraints of subsystem. Then, two sub-systems are iteratively solved for the worst case:

Step 1: Initialize global variable $F_{p,0,couple}$, $F_{p,0,gas}$, $\lambda'_{p,1}$, $\lambda_{p,0}$, penalty factors τ and $c_{p,0}$. Set iteration index $r = 1$. Set the convergence thresholds ε. Set $\alpha_1 = 1$;

Step 2: Solve (52) with given $F_{p,r,couple}$ and obtain the optimal solution $F_{p,r,grid}$;

Step 3: Solve (53) with given $F_{p,r,grid}$ and obtain the optimal solution $F_{p,r,gas}$;

Step 4: Calculate the Lagrange multipliers $\lambda_{p,r}$ by $\lambda'_{p,r}$, $F_{p,r,grid}$ and $F_{p,r,gas}$ in (55), and $c_{p,r}$ is obtained by τ, $\lambda_{p,r}$, $\lambda'_{p,r}$, $F_{p,r,grid}$ and $F_{p,r,gas}$ in (56);

Step 5: If $c_{p,r} < \sigma * c_{p,r-1}$, update α_{r+1}, $F_{p,r+1,couple}$, $\lambda'_{p,r+1}$ by Eq. (57), Eq. (58), Eq. (59), otherwise, set $\alpha_{r+1} = 1$, $F_{p,r+1,couple} = F_{p,r-1,gas}$, $\lambda'_{p,r+1} = \lambda_{p,r-1}$, $c_{p,r} = 1/\sigma * c_{p,r-1}$;

Step 6: If thresholds are met in Eq. (54), the final optimal solution is obtained; Otherwise, go to Step 2.

$$Gap = max\{F_{p,r,grid} - F_{p,r,gas}, F_{p,r,gas} - F_{p,r,couple}\} \quad (54)$$

$$\lambda_{p,r}(t) = \lambda'_{p,r}(t) + \tau[F_{p,r,grid}(t) - F_{p,r,gas}(t)] \quad (55)$$

$$c_{p,r}(t) = \frac{[\lambda'_{p,r}(t) - \lambda_{p,r}(t)]^2}{\tau} + \tau[F_{p,r,gas}(t) - F_{p,r,couple}(t)]^2 \quad (56)$$

$$\alpha_{r+1} = [1 + \sqrt{1 + \alpha_r^2}]/2 \quad (57)$$

$$F_{p,r+1,couple}(t) = F_{p,r,gas}(t) + \frac{\alpha_r - 1}{\alpha_{r+1}}[F_{p,r,gas}(t) - F_{p,r-1,gas}(t)] \quad (58)$$

$$\lambda'_{p,r+1}(t) = \lambda_{p,r}(t) + \frac{\alpha_r - 1}{\alpha_{r+1}}[\lambda_{p,r}(t) - \lambda_{p,r-1}(t)] \quad (59)$$

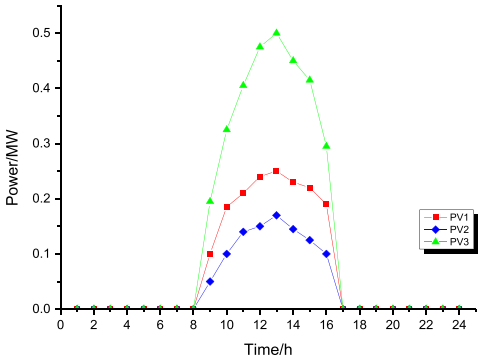

FIGURE 8. Forecasted hourly power of PV.

V. CASE STUDY

In this section, numerical studies are conducted for analyzing the performance of our proposed model, and the effects of the uncertainties and DSM are investigated. The performance of fast-ADMM with restart algorithm is also investigated compared with standard ADMM [18]. In this paper, as shown in Figure 7, the example system includes the IEEE33 node radiation distribution network and a 7-node NG network, which is implemented in YALMIP and solved by Gurobi 7.0.2. The voltage of the balanced node is 12.66kV, and the voltage range of each node is 0.95 p.u∼1.05 p.u. The nodes 14, 16, 31 are connected to three wind turbines (WTs), and the nodes 19, 27, 32 are connected to three photovoltaic (PV) arrays. The hourly forecasted hourly power of PV arrays and WTs are shown in Figure 8 and Figure 9, respectively. The 3, 4, 6, 7 nodes of the NG network are connected to the power network nodes 8, 13, 16, 33 by MT [45]. Besides, the load in node 8, 14, 33 include decentralized AC load taking in 30%, 30% and 40% of total load. For node 24, centralized ice-storage AC is configured to meet the cooling load. The chiller power of centralized ice-storage AC is 250kW, and the capacity of ice-storage tank is 1800kWh. The peak load of centralized ice-storage AC is 500kW, and the total load

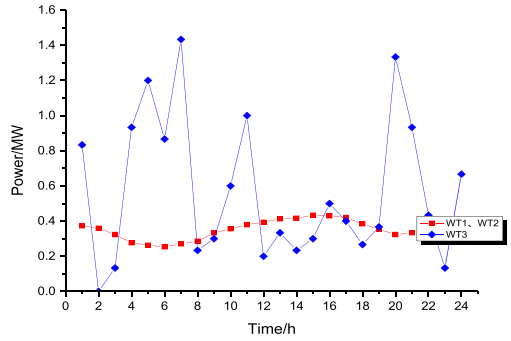

FIGURE 9. Forecasted hourly power of WT.

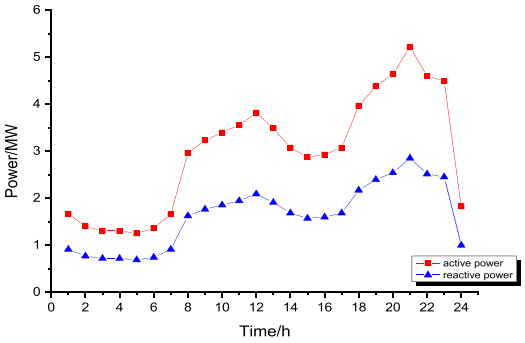

FIGURE 10. Forecasted hourly total load.

is 4020kWh. The total load per hour is shown in Figure 10. The uncertain bounds of DG, electricity load and the NG load forecast data is 10%.

A. OPTIMAL SCHEDULING OF IENG CONSIDERING DSR AND UNCERTAINTY

To verify the proposed model, four cases are considered:

Case1: without considering uncertainty and DSR;
Case2: with only considering uncertainty;
Case3: with only considering DSR;
Case4: with considering uncertainty and DSR.

1) THE EFFECT OF UNCERTAINTIES

The operation costs of four cases are shown in Table 1, and Figure 11 shows the NG consumption of MT. The NG consumption variations in Case2 compared to Case1 are shown in Figure 12 and Figure 13 shows the column variation of NG storage tank where the NG is stored in low electricity price period especially from 0:00 to 8:00, and released in high electricity price period, 12:00-15:00 and 18:00-23:00. Compared to Case 1 and Case 2 in Figure 11 and Figure 13, in which the uncertainty is considered, MT and the NG storage tank are required to absorb more NG to balance the supply and demand. It can be observed in Figure 12 and Table 2 that the consumption of NG of Case2 is larger than the consumption in Case1, and especially in MT4 the NG consumption variation reaches 28.15MBtu (Million Britain Thermal Unit) during scheduling period.

TABLE 1. The operation cost of system.

Case	Case1	Case2	Case3	Case4
NG-side Cost/$	2280	2279	2283	2282
Electricity-side Cost/$	-21190	-16985	-21632	-17443
Total Cost/$	-18910	-14706	-19349	-15161

TABLE 2. The specific natural gas consumption variation in case2 compared with case1 (MBtu).

Time/h	MT1	MT2	MT3	MT4
1	0	-0.003	-0.028	1.438
2	-0.114	0	0	0.566
3	0.110	0	0	0.022
4	0	0	0	-0.069
5	0.359	0.359	0.132	-0.009
6	0.337	0	-0.046	0.106
7	0.337	-0.250	-0.055	0.084
8	0.741	0.637	1.483	2.222
9	0	-0.061	-0.142	0
10	0	0	0.005	0
11	0	0	-0.134	1.872
12	0	0.190	-0.041	0.510
13	0	0	-0.175	1.203
14	-0.499	-0.070	0	1.043
15	-0.023	-0.125	0	0.991
16	0	0	-0.098	1.2668
17	0	0.382	-0.394	0.797
18	0.449	0	0.449	1.673
19	0.427	0	-0.081	0.975
20	0	0.206	0	3.145
21	0.538	0	0.516	0.265
22	0.449	0.449	0	1.796
23	0	0.449	-0.209	0.898
24	-0.223	0	0	1.052
Total	2.89	2.16	1.181	21.85

The power of point of common coupling (PCC) node is shown in Figure 14. The power transferred from the distribution network to main grid is decreasing in Case2 because of the increasing electricity load and decreasing output power of DG in the worst case, which result in the higher costs on the electricity side. In addition, the gas load is decreasing in worst case which result in the lower profits on the NG side. Eventually, the operation costs of IENG in Case2 is higher than that in Case1.

2) THE EFFECT OF DSR

As shown in Figure 15, the ice-storage AC load makes and storages ice in the evening leading to the increase of load from 22:00 to 7:00 of the next day, and in the daytime the ice is melted from 9:00 to 18: 00 leading to load decreasing. The DSR of centralized AC load directly affects the change in the node voltage. The voltage variation of node 24 in Case3 is

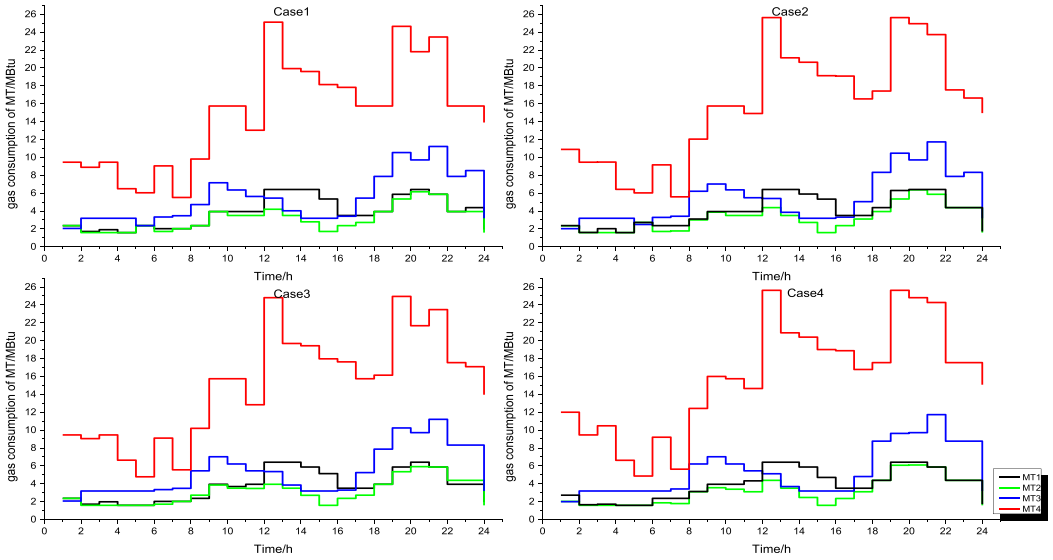

FIGURE 11. Forecasted hourly total load.

TABLE 3. The specific natural gas consumption variation in case3 compared with case1 (MBtu).

Time/h	MT1	MT2	MT3	MT4
1	0	0	0.021	0
2	0	0	0	0.153
3	0.0665	0	0	0
4	0	0	0	0.1445
5	-0.769	-0.771	0.826	-1.251
6	1.371	0	0.0163	0.0537
7	0	0	0	0.0452
8	0	0.359	0.719	0.375
9	0	-0.0814	-0.142	0
10	-0.244	0	-0.147	0
11	0	-0.0366	-0.178	-0.198
12	0	-0.259	-0.082	-0.304
13	0	0	-0.166	-0.242
14	-0.539	-0.084	0	-0.167
15	-0.214	-0.122	0	-0.171
16	0	0	-0.133	-0.204
17	0	0	-0.199	0
18	0	0	0	0.389
19	0	0	-0.299	0.299
20	0	-0.249	0	-0.13
21	0	0	-0.011	0.011
22	0	0.449	0.449	1.796
23	-0.449	0.449	-0.209	1.347
24	0.016	0.003	0	0.0515
Total	-2.133	-0.343	0.478	1.998

shown in Figure 16. The voltage drops during the day due to the decrease of the load consumption and the voltage rises at night due to the increase of the ice-storage AC load.

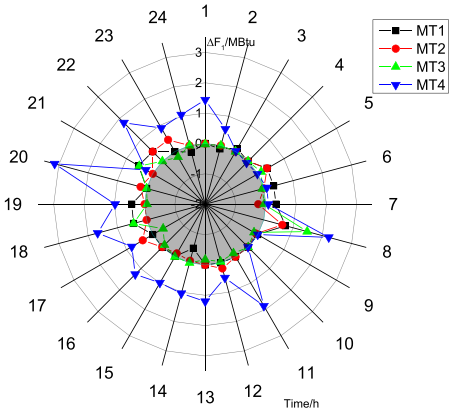

FIGURE 12. The natural gas consumption variation in case2 compared with case1.

Similarly, the decentralized AC load is curtailed. Affected by the centralized ice-storage AC load and decentralized AC load, the power of PCC in Case3 is changed compared with that in Case1, which is shown in Figure 14. The power of PCC, where the power is transferred from the distribution network to the main grid, is decreased during 0:00 to 8:00 because the increasing of the centralized ice-storage AC load is larger than the decreasing load of the decentralized AC load. After 8:00, the power of PCC starts increasing. Besides, the load variation also affects the voltage of the corresponding nodes. The voltage of node 8, 14, 30 is changed because of the DSR of decentralized AC load, and the voltage of node 8 is shown in Figure 17 as an example. Owing to the power transferring from the distribution network to the main grid, the high power of lines could result in high voltage loss, which further lead to high node voltage. Therefore, the voltage of three nodes are decreased due to the decrease of power and

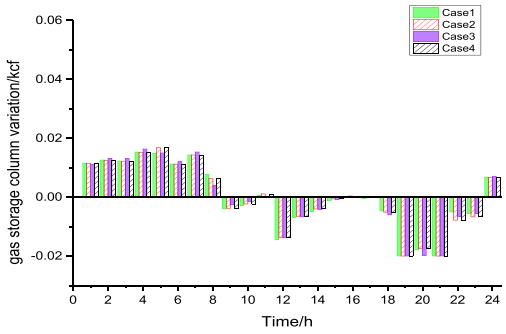

FIGURE 13. The column of natural gas storage tank.

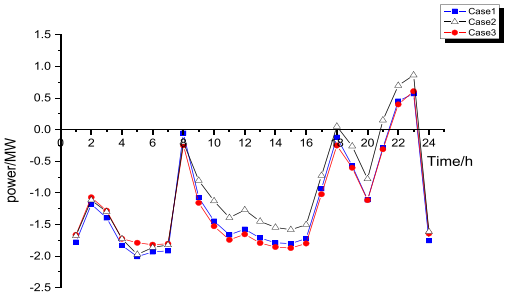

FIGURE 14. The power of PCC.

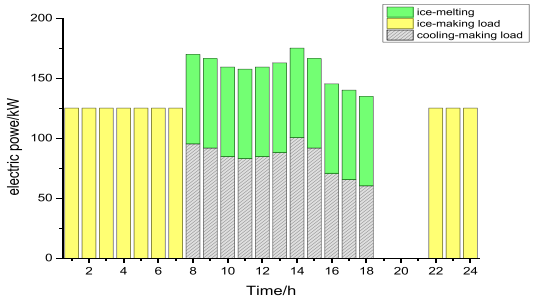

FIGURE 15. Load of ice-storage conditioning.

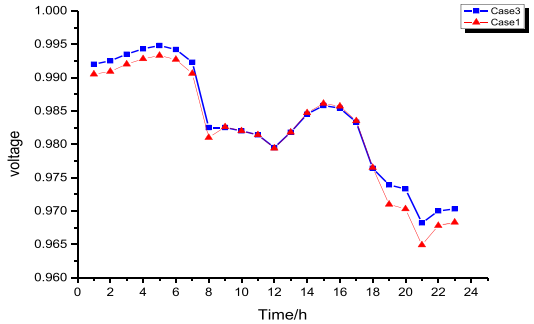

FIGURE 16. The voltage at node 24.

voltage loss during 0:00 to 8:00, and after 8:00 the voltage of these nodes is increased which is raised by the increased of power and voltage loss.

The NG consumption variations in Case3 compared with Case1 are shown in Figure 18 and Table 3. It can be observed

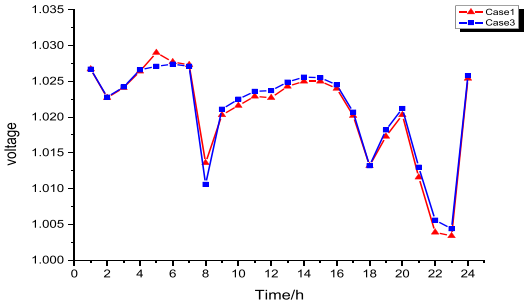

FIGURE 17. The voltage at node 8.

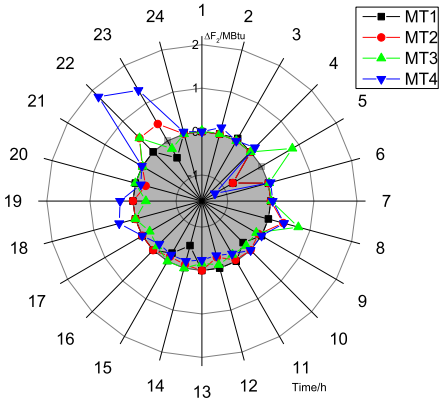

FIGURE 18. The natural gas consumption variation in case3 compared with case1.

that the total NG consumption of Case1 is the same as the entire dispatch cycle in the case of DSR only. Moreover, in Case3 the storage amount is declined from 9:00 to 17:00 comparing with Case1 which leads to increased gas consumption of MT. More NG is stored in low electricity price time from 24:00 to next 8:00, and released in high electricity price time from 18:00 to 23:00, which produce more profits. Despite the slightly increased storage cost, the introducing of DSR decrease the cost of entire system.

B. COMPARISONS ON STANDARD ADMM AND FAST-ADMM WITH RESTART

In this section, costs and the deviations between local variables are given to compare the iteration characteristic of standard ADMM and fast-ADMM with restart. As is shown in Figure 19, the costs in standard ADMM has converged with 25 iterations, and the costs in fast-ADMM with restart has converged with 47 iterations. In contrast, as shown in Figure 20, convergence accuracy in fast-ADMM with restart meet the convergence conditions with only 53 iterations. However, convergence accuracy in standard ADMM cannot reach the convergence conditions even after 80 iterations. Therefore, the fast-ADMM with restart algorithm has higher convergence accuracy than standard ADMM within limited iteration times.

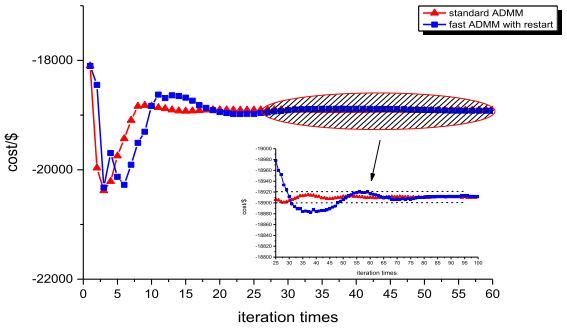

FIGURE 19. Costs of iteration.

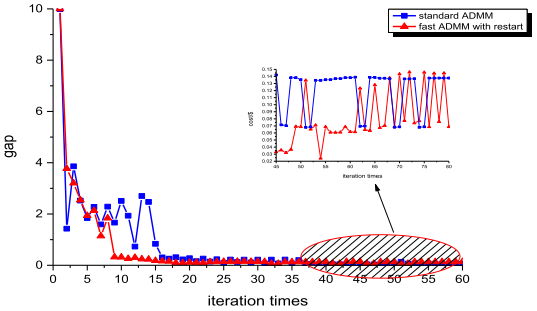

FIGURE 20. The biggest deviation between local variables.

VI. CONCLUSION

This paper proposes an IENG system model at a distributed level and provides a day-ahead scheduling framework. In this model, both the electric network and the linearized NG network model are established. Based on the worst case obtained by C&CG algorithm and fast-ADMM with restart algorithm, the scheduling scheme is optimized under the day-ahead scheduling framework. Case studies with our theory show that:

1) With the scheduling framework, the complement characteristic of the decentralized AC load and the centralized AC load are considered, and the total electric load is curtailed which reduces the operation costs;
2) The uncertainties, especially the uncertainties from the NG, are considered in this paper, which indicates the robustness of the proposed scheduling scheme obtained by solving TSRO problem. In other words, it guarantees the feasibility and economy in the worst case.
3) We implement the fast-ADMM with restart algorithm in this design. Compared to the standard ADMM algorithm, the fast-ADMM with restart algorithm has higher convergence accuracy within limited iteration.

REFERENCES

[1] M. Urbina and Z. Li, "A combined model for analyzing the interdependency of electrical and gas systems," in *Proc. IEEE North Amer. Power Symp. (NAPS)*, Sep./Oct. 2007, pp. 468–472.

[2] T. Groth and B. Scholtens, "A comparison of cost-benefit analysis of biomass and natural gas CHP projects in Denmark and The Netherlands," *Renew. Energy*, vol. 86, pp. 1095–1102, Feb. 2017.

[3] C. Sahin, Z. Li, M. Shahidehpour, and I. Erkmen, "Impact of natural gas system on risk-constrained midterm hydrothermal scheduling," *IEEE Trans. Power Syst.*, vol. 26, no. 2, pp. 520–531, May 2010.

[4] N. Zhang, Z. Hu, B. Shen, G. He, and Y. Zheng, "An integrated source-grid-load planning model at the macro level: Case study for China's power sector," *Energy*, vol. 126, pp. 231–246, May 2017.

[5] X. Xu, H. Jia, D. Wang, D. C. Yu, and H.-D. Chiang, "Hierarchical energy management system for multi-source multi-product microgrids," *Renew. Energy*, vol. 78, pp. 621–630, Jun. 2015.

[6] Y. Hu, Z. Bie, T. Ding, and Y. Lin, "An NSGA-II based multi-objective optimization for combined gas and electricity network expansion planning," *Appl. Energy*, vol. 167, pp. 280–293, Apr. 2016.

[7] F. Liu, Z. Bie, S. Liu, and T. Ding, "Day-ahead optimal dispatch for wind integrated power system considering zonal reserve requirements," *Appl. Energy*, vol. 188, pp. 399–408, Feb. 2017.

[8] C. Shao, M. Shahidehpour, X. Wang, X. Wang, and B. Wang, "Integrated planning of electricity and natural gas transportation systems for enhancing the power grid resilience," *IEEE Trans. Power Syst.*, vol. 32, no. 6, pp. 4418–4429, Nov. 2017.

[9] I. G. Sardou, M. E. Khodayar, and M. T. Ameli, "Coordinated operation of natural gas and electricity networks with microgrid aggregators," *IEEE Trans. Smart Grid*, vol. 9, no. 1, pp. 199–210, Jan. 2018.

[10] X. Zhang, G. G. Karady, and S. T. Ariaratnam, "Optimal allocation of CHP-based distributed generation on urban energy distribution networks," *IEEE Trans. Sustain. Energy*, vol. 5, no. 1, pp. 246–253, Jan. 2014.

[11] X. Zhang, L. Che, M. Shahidehpour, A. Alabdulwahab, and A. Abusorrah, "Electricity-natural gas operation planning with hourly demand response for deployment of flexible ramp," *IEEE Trans. Sustain. Energy*, vol. 7, no. 3, pp. 996–1004, Jul. 2016.

[12] J. Qiu *et al.*, "Multi-stage flexible expansion co-planning under uncertainties in a combined electricity and gas market," *IEEE Trans. Power Syst.*, vol. 30, no. 4, pp. 2119–2129, Jul. 2015.

[13] X. Zhang, L. Che, and M. Shahidehpour, "Long-term expansion planning of integrated electricity and natural gas transportation infrastructures," in *Proc. IEEE Power Energy Soc. Gen. Meeting*, Jul. 2015, pp. 1–5.

[14] C. A. Saldarriaga, R. A. Hincapie, and H. Salazar, "A holistic approach for planning natural gas and electricity distribution networks," *IEEE Trans. Power Syst.*, vol. 28, no. 4, pp. 4052–4063, Nov. 2013.

[15] Y. Hu, Z. Bie, G. Li, T. Ding, and H. Lian, "Integrated planning of natural gas network and composite power system," *Proc. CSEE*, vol. 37, no. 1, pp. 45–53, 2017.

[16] Z. Wei, S. Chen, G. Sun, D. Wang, Y. Sun, and H. Zang, "Probabilistic available transfer capability calculation considering static security constraints and uncertainties of electricity–gas integrated energy systems," *Appl. Energy*, vol. 167, pp. 305–316, Apr. 2016.

[17] Z. Qiao, Q. Guo, H. Sun, Z. Pan, Y. Liu, and W. Xiong, "An interval gas flow analysis in natural gas and electricity coupled networks considering the uncertainty of wind power," *Appl. Energy*, vol. 201, pp. 343–353, Sep. 2017.

[18] C. He, L. Wu, T. Liu, and M. Shahidehpour, "Robust co-optimization scheduling of electricity and natural gas systems via ADMM," *IEEE Trans. Sustain. Energy*, vol. 8, no. 2, pp. 658–670, Apr. 2017.

[19] X. Zhang, M. Shahidehpour, A. Alabdulwahab, and A. Abusorrah, "Hourly electricity demand response in the stochastic day-ahead scheduling of coordinated electricity and natural gas networks," *IEEE Trans. Power Syst.*, vol. 31, no. 1, pp. 592–601, Jan. 2016.

[20] M. Chaudry, J. Wu, and N. Jenkins, "A sequential Monte Carlo model of the combined GB gas and electricity network," *Energy Policy*, vol. 62, pp. 473–483, Nov. 2013.

[21] D. Neves, M. C. Brito, and C. A. Silva, "Impact of solar and wind forecast uncertainties on demand response of isolated microgrids," *Renew. Energy*, vol. 87, pp. 1003–1015, Mar. 2016.

[22] P. Faria, T. Soares, Z. Vale, and H. Morais, "Distributed generation and demand response dispatch for a virtual power player energy and reserve provision," *Renew. Energy*, vol. 66, pp. 686–695, Jun. 2014.

[23] Y. Bai, J. Wu, T. Xiong, J. Xu, and J. Huang, "Optimal dispatch of air conditioning load in micro-grid considering the consumers' comfort," in *Proc. IEEE Int. Conf. Smart Grid Commun.*, Nov. 2016, pp. 395–398.

[24] Z. Bao, Q. Zhou, Z. Yang, Q. Yang, L. Xu, and T. Wu, "A multi time-scale and multi energy-type coordinated microgrid scheduling solution—Part I: Model and methodology," *IEEE Trans. Power Syst.*, vol. 30, no. 5, pp. 2257–2266, Sep. 2015.

[25] G. A. O. Ciwei, L. I. Qianyu, and L. I. Yang, "Bi-level optimal dispatch and control strategy for air-conditioning load based on direct load control," *Proc. CSEE*, vol. 34, no. 10, pp. 1546–1555, 2014.
[26] M. E. Baran and F. F. Wu, "Network reconfiguration in distribution systems for loss reduction and load balancing," *IEEE Trans. Power Del.*, vol. 4, no. 2, pp. 1401–1407, Apr. 1989.
[27] H.-G. Yeh, D. F. Gayme, and S. H. Low, "Adaptive VAR control for distribution circuits with photovoltaic generators," *IEEE Trans. Power Syst.*, vol. 27, no. 3, pp. 1656–1663, Aug. 2012.
[28] Z. Wang, B. Chen, J. Wang, M. M. Begovic, and C. Chen, "Coordinated energy management of networked microgrids in distribution systems," *IEEE Trans. Smart Grid*, vol. 6, no. 1, pp. 45–53, Jan. 2015.
[29] Z. Wang, B. Chen, J. Wang, and J. Kim, "Decentralized energy management system for networked microgrids in grid-connected and islanded modes," *IEEE Trans. Smart Grid*, vol. 7, no. 2, pp. 1097–1105, Mar. 2016.
[30] H. M. Markowitz and A. S. Manne, "On the solution of discrete programming problems," *Econometrica*, vol. 25, no. 1, pp. 84–110, 1957.
[31] Y. Liu, S. Gao, X. Zhao, C. Zhang, and N. Zhang, "Coordinated operation and control of combined electricity and natural gas systems with thermal storage," *Energies*, vol. 10, no. 7, p. 917, 2017.
[32] M. Kalantar and S. M. Mousavi G, "Dynamic behavior of a stand-alone hybrid power generation system of wind turbine, microturbine, solar array and battery storage," *Appl. Energy*, vol. 87, no. 10, pp. 3051–3064, 2010.
[33] N. Lu and D. P. Chassin, "A state-queueing model of thermostatically controlled appliances," *IEEE Trans. Power Syst.*, vol. 19, no. 3, pp. 1666–1673, Aug. 2004.
[34] D. Wang, M. Fan, and H. Jia, "User comfort constraint demand response for residential thermostatically-controlled loads and efficient power plant modeling," *Proc. CSEE*, vol. 34, no. 13, pp. 2071–2077, 2014.
[35] H.-J. Chen, D. W. P. Wang, and S.-L. Chen, "Optimization of an ice-storage air conditioning system using dynamic programming method," *Appl. Thermal Eng.*, vol. 25, nos. 2–3, pp. 461–472, 2005.
[36] G. Fang, X. Liu, and S. Wu, "Experimental investigation on performance of ice storage air-conditioning system with separate heat pipe," *Experim. Thermal Fluid Sci.*, vol. 33, no. 8, pp. 1149–1155, 2009.
[37] Y. He, M. Shahidehpour, Z. Li, C. Guo, and B. Zhu, "Robust constrained operation of integrated electricity-natural gas system considering distributed natural gas storage," *IEEE Trans. Sustain. Energy*, to be published, doi: 10.1109/TSTE.2017.2764004.
[38] T. Li, M. Eremia, and M. Shahidehpour, "Interdependency of natural gas network and power system security," *IEEE Trans. Power Syst.*, vol. 23, no. 4, pp. 1817–1824, Nov. 2008.
[39] L. Bai, F. Li, H. Cui, T. Jiang, H. Sun, and J. Zhu, "Interval optimization based operating strategy for gas-electricity integrated energy systems considering demand response and wind uncertainty," *Appl. Energy*, vol. 167, pp. 270–279, Apr. 2016.
[40] M. Chaudry, N. Jenkins, M. Qadrdan, and J. Wu, "Combined gas and electricity network expansion planning," *Appl. Energy*, vol. 113, pp. 1171–1187, Jan. 2014.
[41] C. Zhang, Y. Xu, Z. Y. Dong, and J. Ma, "Robust operation of microgrids via two-stage coordinated energy storage and direct load control," *IEEE Trans. Power Syst.*, vol. 32, no. 4, pp. 2858–2868, Jul. 2017.
[42] B. Zeng and L. Zhao, "Solving two-stage robust optimization problems using a column-and-constraint generation method," *Oper. Res. Lett.*, vol. 41, no. 5, pp. 457–461, 2013.
[43] S. Boyd, N. Parikh, E. Chu, B. Peleato, and J. Eckstein, "Distributed optimization and statistical learning via the alternating direction method of multipliers," *Found. Trends Mach. Learn.*, vol. 3, no. 1, pp. 1–122, Jan. 2011.
[44] T. Goldstein, B. O'Donoghue, S. Setzer, and R. Baraniuk, "Fast alternating direction optimization methods," *Siam J. Imag. Sci.*, vol. 7, no. 3, pp. 1588–1623, 2014.
[45] X. Jin, Y. Mu, H. Jia, J. Wu, X. Xu, and X. Yu, "Optimal day-ahead scheduling of integrated urban energy systems," *Appl. Energy*, vol. 180, pp. 1–13, Oct. 2016.

JIAN CHEN (M'16) received the B.S. degree in electrical engineering from Shandong University, Jinan, China, in 2009, and the Ph.D. degree in electrical engineering from Tianjin University, Tianjin, China, in 2014.

He was with Nanyang Technological University as a Research Fellow from 2015 to 2016. He is currently a Lecturer with the Key Laboratory of Power System Intelligent Dispatch and Control of Ministry of Education, Shandong University. His research interests include distributed generations, microgrid optimization, and integrated energy system.

WEITONG ZHANG (S'17) received the B.S. degree from the China University of Petroleum, Qingdao, China, in 2016. He is currently pursuing the M.S. degree with the School of Electrical Engineering, Shandong University, China. His research interests include microgrid optimization and integrated energy system.

YICHENG ZHANG (S'15) received the M.S. degree from the University of Science and Technology of China in 2014. He is currently pursuing the Ph.D. degree with Nanyang Technological University, Singapore. His current research interests include optimization method, model-based fault diagnosis, smart grid, and intelligent transportation systems.

GUANNAN BAO received the B.S. degree in electrical engineering from Zhejiang University, Hangzhou, China, in 2010, and the M.S. degree in electrical engineering from Tsinghua University, Beijing, China, in 2012. She is currently an Engineer with the State Grid Shandong Electric Power Dispatching and Control Center, Jinan, China. Her current research interests include power system dispatching and maintenance schedule management.